Wang F, Zhao O, Young B. Flexural behaviour and strengths of press-braked S960 ultra-high strength steel channel section beams. Engineering Structures. 2019;200:109735.

Flexural behaviour and strengths of press-braked S960 ultra-high strength steel channel section beams

Fangying Wang[a], Ou Zhao[a,*], Ben Young[b]

[a] *School of Civil and Environmental Engineering, Nanyang Technological University, Singapore*

[b] *Department of Civil and Environmental Engineering, The Hong Kong Polytechnic University, Hong Kong, China. (Formerly, Department of Civil Engineering, The University of Hong Kong, Pokfulam Road, Hong Kong, China.)*

[*] Corresponding author, Email: ou.zhao@ntu.edu.sg

Abstract

A thorough experimental and numerical study of the flexural behaviour and strengths of press-braked S960 ultra-high strength steel (UHSS) channel section beams bent about the minor principal axes is reported in this paper. The experimental study was conducted on eight different ultra-high strength steel plain channel sections, and included measurements on the material flat and corner properties and initial local geometric imperfections of the beam specimens and 20 four-point bending tests performed about the minor principal axes in both the 'u' and 'n' orientations. A complementary numerical investigation was then conducted, where finite element (FE) models were firstly developed and validated against the experimental results, followed by parametric studies carried out to acquire further numerical data over a broader range of cross-section dimensions. It is worth noting that the existing design codes for steel structures, as established in Europe, America and Australia/New Zealand, are only applicable to those with material grades up to S690 (or S700 for Eurocode) and cannot be directly used for S960 UHSS structural members. In the present study, the applicability of the

codified design provisions and formulations for flexural members to the examined S960 UHSS channel section beams was evaluated, based on the ultimate moments derived from structural testing and numerical modelling. The quantitative evaluation results generally revealed that the current European code provides overall consistent and precise flexural strength predictions for Class 1 and Class 2 S960 UHSS channel sections in minor-axis bending, but leads to a high level of inaccuracy (scatter and conservatism) for the design of their Class 3 and Class 4 counterparts, whilst the American specification and Australian/New Zealand standard result in scattered and excessively underestimated design flexural strengths, except for the cases of slender S960 UHSS channel section beams in 'u'-orientation bending.

Keywords: Cross-section bending moment resistances; Design standards; Four-point bending tests; Numerical modelling; Plain channel sections; Press-braked; S960 ultra-high strength steel; Slenderness limits

1. Introduction

High strength steels (HSS), possessing superior strength-to-weight ratios over normal strength mild steels, provide the possibility of designing structural members and joints with reduced dimensions and weights and lead to optimal designs of structures [1,2]. Ease of off-site fabrication as well as on-site erection and assembly of structural members can thus be achieved, marking HSS as an ideal construction material for both heavy (long-span and high-rise) [3,4] and light gauge [5] structures. Ultra-high strength steel (UHSS) Grade S960, with the nominal yield stress of 960 MPa, has already become commercially available in the past decade. It is currently being extensively used in the automotive industry, for example, for the fabrication of chassis of container trailers and lifting systems of truck mounted cranes. However, its applications in structural engineering remain scarce, primarily owing to lack of codified design rules, as the established international standards only cover the design of high strength steel structures with material grades up to S690 (or S700). This has thus prompted research, aimed at examining the structural behaviour of different types of S960 UHSS members, quantifying their load-carrying capacities, and developing precise design rules for them. Specifically, Li et al. [4] and Shi et al. [6] conducted stub column tests on S960 UHSS welded box sections and I-sections to examine their cross-sectional behaviour and resistances in pure compression, while the structural performance and load-carrying capacities of cold-formed S960 UHSS circular, rectangular, and square hollow section stub columns were experimentally investigated by Ma et al. [7]. A series of long column tests were performed on S960 UHSS welded I-sections [8] and box sections [9] to examine their overall stability. Ma et al. [10] conducted four-point bending tests on cold-formed S960 UHSS tubular section beams to investigate their in-plane bending behaviour and resistances. Overall, the brief review generally indicated that previous studies mainly focused on doubly symmetric S960 UHSS I- and tubular section compression and flexural members. To date, the structural behaviour of S960 UHSS members of non-doubly symmetric cross-section profiles has not been examined.

As part of an ongoing research programme on the static and cyclic behaviour of non-doubly symmetric S960 UHSS angle and channel section structural members, the present investigation focuses on the flexural performance and strengths of press-braked S960 UHSS channel section beams, underpinned by a thorough testing and numerical modelling programme. The testing programme was carried out on eight plain channel sections, and included measurements on the material properties and initial local geometric imperfections of the specimens as well as 20 four-point bending tests conducted about the minor principal axes in both the ‘u’ and ‘n’ orientations. The experimental results were utilised in a numerical modelling programme for the validation of finite element (FE) models, and parametric studies were subsequently performed, based on the validated FE models, to acquire further numerical data over a broader range of cross-section sizes. The derived experimental and numerical data was adopted to assess the applicability of the Eurocode Class 2 and 3 slenderness limits as well as the design formulations established in the European code EN 1993-1-12 [11], North American specification AISI S100 [12], Australian/New Zealand standard AS/NZS 4600 [13] for S690 HSS channel section flexural members to the design of their S960 UHSS counterparts.

2. Experimental investigation

2.1. Press-braked channel section beam specimens

All the test specimens were fabricated (press-braked) from the same batch of ultra-high strength steel grade S960 sheets with the nominal material thickness of 6 mm. The fabrication process is shown Fig. 1, where the S960 UHSS sheet is firstly cut to size, then positioned on a V-shaped die, and finally press-braked into the required cross-section profile using an appropriate punch. Particular attention needs to be paid to the selection of punches for press-braking S960 ultra-high strength steel characterising brittle nature. The minimum punch nose radii (R_p) are respectively required to be 3.0 and 2.5 times the sheet thickness for press-braking along and perpendicular to the sheet rolling direction [14]. Failure to comply with these requirements may result in cracks along the bend line of the specimen [15], which would, of course, has a detrimental effect on the member structural performance. In the present study, press-braking was all performed with the direction perpendicular to the sheet rolling direction, using a punch with the nose radius of 15 mm (i.e. 2.5 times the sheet thickness), leading to the nominal inner radii of the press-braked channel section beams equal to 15 mm.

A total of eight plain channel sections (C 70×40×6, C 80×45×6, C 80×55×6, C 100×45×6, C 100×60×6, C 120×45×6, C 120×70×6 and C 120×90×6) were fabricated and used in the present experimental programme. The cross-section identifier is composed of a letter ‘C’ representing a channel section and the nominal cross-section dimensions in millimetre, i.e. outer web width B_w × outer flange width B_f × wall thickness t (see Fig. 2). Each beam specimen was labelled by its cross-section identifier and bending orientation, with letters ‘u’ and ‘n’ respectively representing minor-axis bending in the ‘u’ and ‘n’ orientations. A letter ‘R’ is used for the repeated tests. Measurements on the geometric dimensions of each beam specimen were carefully taken, with the average measured key parameters reported in Table 1.

2.2. Material properties

Tensile flat and corner coupon tests were undertaken to obtain the material properties of the flat portions and corners of the examined press-braked S960 UHSS channel sections. Given that all the channel sections were press-braked from the same batch of S960 UHSS sheets using the same set of punch and die, the variation of the material properties among different cross-sections was deemed to be negligible. Tensile coupons were thus extracted from two representative channel sections C 70×40×6 and C 120×90×6 in the longitudinal direction. Two flat coupons and one corner coupon were machined from each examined channel section at the locations shown in Fig. 2. Moreover, one flat coupon was also cut from the S960 UHSS virgin sheet in the transverse direction – see Fig. 1. The coupon specimens extracted from channel sections were labelled by the corresponding cross-section identifiers and locations within the cross-sections (with ‘W’, ‘F’ and ‘C’ representing webs, flanges and corners of the channel sections, respectively), while the tensile coupon cut from the virgin sheet was labelled as ‘VS’. All the coupon specimens were prepared in compliance with the dimension requirements given in ASTM E8M-15 [16], with a parallel width equal to 12 mm and a gauge length of 50 mm. Fig. 3 displays the flat and corner tensile coupon test setups, where two strain gauges are attached longitudinally to the coupon at mid-height to capture the tensile strains and a calibrated extensometer is mounted onto the coupon to record the elongation over the 50 mm gauge length. All the coupon specimens were tested in an INSTRON 250 kN testing machine, driven by displacement control, with an initial loading rate of 0.05 mm/min up to the nominal yield stress of 960 MPa and a higher rate of 0.4 mm/min thereafter. During the tensile coupon tests, static drops were executed by pausing the testing machine for 100 s near the nominal yield stress and ultimate tensile stress, which allows stress relaxation to take place at these two points. The static measured stress–strain curves of the flat and corner coupons were derived following the procedures described in Huang and Young [17], and presented in Fig. 4, whilst the key measured material properties are summarised in Table 2, where E is Young's modulus, f_y is the yield stress, f_u is the ultimate stress, f_u/f_y is the material ultimate-to-yield stress ratio, and ε_u and ε_f correspond to the strains at the ultimate stress and fracture, respectively. It is evident in Fig. 4 that both the flat and corner coupons display relatively rounded material responses with no obvious yield plateaus and sharply defined yield stresses, and the corresponding 0.2% proof stresses are thus given as the material yield stresses [7,10,15,17–19] in Table 2.

2.3. Initial local geometric imperfections

Initial local geometric imperfections were measured on the S960 UHSS channel section beam specimens prior to the four-point bending tests, with the procedures and setup being in line with those recommended by Schafer and Peköz [20]. The measurement setup is shown in Fig. 5, where the beam specimen is mounted on the table of a CNC router and three linear variable displacement transducers (LVDT), with their tips pointing at the three constituent plate elements (one internal web and two outstand flanges), are used to record the local deviations along the centrelines. For each plate element, the measured data points from the LVDT were fitted by a linear regression line, with the initial local geometric imperfection amplitude taken as the largest derivation from the linear regression line to the original measured data points [21–25], as reported in Table 1, where ω_w, ω_{f1} and ω_{f2} respectively denote the initial local geometric imperfection amplitudes of the internal web and two outstand flanges, whilst the initial local geometric imperfection amplitude of the beam specimen ω_0 is given as the maximum of ω_w, ω_{f1} and ω_{f2}. Figs 6(a) and 6(b) show the measured initial local geometric imperfection distributions of the three constituent plate elements (one internal web and two outstand flanges) for typical press-braked S960 UHSS channel section beam specimens C 80×45×6-u and C 80×45×6-n.

2.4. Four-point bending tests

A total of 20 press-braked S960 UHSS channel section beam specimens was tested in the four-point bending configuration, with the aim of investigating their in-plane flexural behaviour and resistances under constant bending moments. Specifically, for each of the eight examined channel sections, two geometrically identical specimens were prepared and then bent about the cross-section minor principal axis in the 'u' and 'n' orientations, which respectively induce compression and tension at the tip of the outstand flange, as depicted in Figs 7(a) and 7(b); moreover, repeated tests were also performed on two representative channel sections (C 70×40×6 and C 120×70×6) in both the 'u' and 'n' orientations. All the beam specimens were tested in an INSTRON 2000 kN testing machine employing the four-point bending configuration [26–29], as shown in Fig. 8, where the beam specimen is simply supported between two roller supports, located 50 mm away from the specimen end faces, and loaded at two points, with each positioned at a distance of 150 mm from the mid-span of the beam specimen (i.e. the length of the constant moment span L_0 is equal to 300 mm). Given that the lengths of all the tested S960 UHSS channel section beam specimens are equal to 1000 mm, the resulting flexural spans between the two end steel rollers L_f are 900 mm, with the span-to-height ratios of the examined beam specimens falling within the range between 10.0 and 22.5, which ensures that all the beam specimens fail by in-plane flexure with negligible influence from shear. To mitigate against local bearing and crushing failure at the supports and loading points, underpinning bolts were inserted between the inner faces of the flanges at these positions and stiffening plates were also clamped onto the outer faces of the flanges by using G-clamps. During testing, three line transducers were vertically positioned at the mid-span and two loading points to measure the deflections of the specimen at the three locations, while two LVDTs were horizontally positioned at the end rollers to monitor any longitudinal movements of the supports. All the tests were displacement controlled with a constant loading rate of 1.5 mm/min, paused for 100 s near the ultimate moment levels to attain the static moments [17–19,30], and terminated once the moments dropped to 85% of the ultimate moments or levelled off but with excessive curvatures of 1.5 m^{-1} reached.

2.5. Test results

All the tested press-braked S960 UHSS channel section beams failed within the constant moment spans. Specifically, the beam specimens bent in the ‘u’ orientation exhibited visible outward local buckling of the flanges, with a typical failed specimen C 120×90×6-u displayed in Fig. 9, while the beam specimens in ‘n’-orientation bending showed significant in-plane deformations, though the local buckling failure modes were not as visible as their ‘u’-orientation counterparts, with a typical failed specimen C 80×45×6-n presented in Fig. 10. The full ranges of the moment–curvature curves of the tested press-braked S960 UHSS channel section beams bent about the minor principal axes in the 'u' and 'n' orientations are respectively displayed in Figs 11(a) and 11(b), where the curvature κ of the constant moment span is derived from Eq. (1) [28], based on the vertical deflections at the loading points and mid-span (denoted as D_L and D_M, respectively) recorded by the line transducers. It can be seen from Fig. 11 that the difference between the moment–curvature curves measured from each set of the repeated tests is rather small, demonstrating the reliability of the tests. The key experimental results are presented in Table 3, including the ultimate moment $M_{u,test}$, the curvature at the ultimate moment κ_f, the ratios of $M_{u,test}/M_{pl}$ and $M_{u,test}/M_{el}$, where M_{pl} and M_{el} correspond to the cross-section plastic and elastic moment resistances, given as the products of the material yield stress and the plastic and elastic section moduli W_{pl} and W_{el}, respectively, which are determined about the plastic neutral axis (PNA) and elastic neutral axis (ENA) along the minor principal axis direction (see Fig. 7). It is worth noting that channel section beams subjected to 'u'-orientation bending are more vulnerable to local buckling, and thus exhibit less ductile flexural behaviour with steeper post-ultimate moment–curvature responses and lower ultimate moments in comparison with those derived from the same channel section beams in 'n'-orientation bending.

$$\kappa = \frac{8\left(D_M - D_L\right)}{4\left(D_M - D_L\right)^2 + L_0^2} \tag{1}$$

3. Numerical study

3.1. Development of FE models

A complementary numerical study of press-braked S960 UHSS channel section beams was carried out employing the nonlinear FE analysis package ABAQUS [31]. The FE model of each test specimen was developed, based on its measured geometric dimensions and using the S4R shell element [15,19,21–23]. The mesh size and density were determined following a prior mesh sensitivity study considering both the numerical accuracy and computational efficiency. A uniform mesh with the element length and width both equal to the cross-section thickness t was adopted for the flat regions of the channel section beam FE models, while a finer mesh with at least 10 elements was utilised to discretise the corners of the modelled channel sections. The engineering stress–strain curves, as measured from the tensile flat and corner coupon tests, were first converted into the true stress–true plastic strain curves, and then assigned to the respective regions of the channel section beam FE models.

Initial local geometric imperfections were included into the FE models for accurately capturing the physical in-plane flexural responses observed in the tests. The initial local geometric imperfection distribution pattern of each beam FE model was assumed to be of the first elastic local buckling mode shape in four-point bending. Five imperfection amplitudes – the measured values ω_0 and four fractions of the cross-section thickness (t/100, t/50, t/25 and t/10) – were employed to scale the respective imperfection distribution profiles, aimed at examining the sensitivity of the developed beam FE models to the local imperfection amplitudes. Given that membrane residual stresses are rather small in press-braked (cold-formed) steel sections and the examined in-plane flexural behaviour was also insensitive to membrane residual stresses, explicit measurements and modelling of membrane residual stresses in press-braked S960 UHSS channel section beams were both not carried out.

The tested channel section beams were strengthened by means of stiffening plates (with the lengths of 90 mm) at the two loading points and two supports, and these four strengthened portions were respectively set as rigid bodies in the beam FE models. Suitable boundary conditions were applied to the four rigid bodies. Specifically, the rigid body at one end support was allowed for rotation about the centreline of its bottom face as well as translation along the longitudinal direction of the beam FE model (i.e. model length direction), whilst the rigid body at the other end support was only allowed to rotate about the centreline of its bottom face, for the purpose of replicating the simply-supported boundary condition used in the tests. The four-point bending configuration was then achieved by allowing each rigid body at the loading point to rotate about the centreline of its top face and translate in both the longitudinal and vertical directions. Upon development of the press-braked S960 UHSS channel section beam FE models, nonlinear static analyses were conducted by applying the same vertical displacements at the two loading points to mimic the displacement-controlled loading scheme used in the experiments.

3.2. Validation of FE models

Validation of the developed S960 UHSS channel section beam FE models was made by comparing the numerically acquired ultimate moments, moment–curvature curves and failure modes against the test observations presented in Section 2.5. The numerical to experimental ultimate moment ratios $M_{u,FE}/M_{u,test}$ for the five examined imperfection amplitudes are reported in Table 4, revealing that all the five imperfection amplitudes generally yield satisfactory agreement between the numerical and experimental ultimate moments, whilst the most accurate yet still safe predictions of the test ultimate moments are attained when the local imperfection amplitudes of t/10 are adopted. It can also be observed that the numerical ultimate moments derived from the channel section beam FE models bent in the 'u' orientation are more sensitive to the local imperfection amplitudes, due to the fact that the 'u'-orientation bending cases, with the tips of the outstand flanges in compression, are more susceptible to local buckling.

Comparisons between the experimental and numerical moment–curvature curves for typical examined S960 UHSS channel sections C 80×55×6 and C 100×45×6 in bending about the minor principal axes in both the ‘u’ and ‘n’ orientations are presented in Fig. 12, where the experimental flexural responses are precisely replicated by their numerical counterparts. Good agreement was also obtained for the deformed failure modes; typical examples are displayed in Figs 9 and 10. In summary, the developed FE models are capable of replicating the in-plane flexural behaviour of the tested press-braked S960 UHSS channel section beam specimens, and thus considered to be validated.

3.3. Parametric studies

The validated FE models were employed in the parametric studies to generate further numerical data on press-braked S960 UHSS channel section beams over a broader range of cross-section geometric sizes. Tables 5 and 6 summarise the cross-section sizes of the modelled channel section beams bent in the ‘u’ and ‘n’ orientations, respectively, considering a wide variety of practically used cross-section aspect ratios from 1.0 to 3.0 [32] and also covering all the four classes of cross-sections defined in the European code EN 1993-1-12 [11]. The lengths of all the modelled channel section beams were fixed at 1000 mm, with the constant moment spans located over the central 300 mm. In the present parametric studies, the stress–strain curves of channel section C 120×90×6 were employed, whilst the initial local geometric imperfection amplitudes were taken as 1/10 of the wall thicknesses of the modelled channel sections. A total of 113 FE simulations on press-braked S960 UHSS channel section beams were completed, with 55 for the ‘u’-orientation bending cases and 58 for the ‘n’-orientation bending cases.

4. Evaluation of current design standards

4.1. EN 1993-1-12 (EC3)

4.1.1. General

The current European code EN 1993-1-12 [11] for high strength steels covers the design of hot-rolled and welded steel structural members with material grades up to S700. Regarding the design of beam members susceptible to in-plane bending failure, EN 1993-1-12 [11] adopts the same cross-section classification approach and effective width expression as those outlined in EN 1993-1-1 [33] for normal strength steels. A cross-section is classified according to the least favourable class of its constituent plate elements, while classification of each plate element is made by comparing its flat width-to-thickness ratio against the EC3 prescribed slenderness limits. There are a total of four classes of cross-sections defined in the European codes EN 1993-1-12 [11] and EN 1993-1-1 [33]. Class 1 and Class 2 sections, also termed plastic sections, can obtain the plastic moment capacities (M_{pl}=$W_{pl}f_y$) at failure. Class 3 sections, also termed elastic sections, are capable of developing the elastic moment capacities (M_{el}=$W_{el}f_y$) at failure. Class 4 sections, also termed slender sections, are more prone to local buckling and fail before the material yield stresses are reached, with the cross-section bending moment resistances at failure limited to the effective moment capacities (M_{eff}=$W_{eff}f_y$), where W_{eff} is determined based on the effective area of the cross-section in bending, consisting of the full areas of the corners, the full areas of the tensile flat portions and the effective areas of the compressive flat portions. The effective width of the compressive portion of the plate element b_{eff} is calculated as a product of the full width of the compression portion of the plate element b_c and a reduction factor for plate buckling ρ, as derived from the effective width expression given by Eq. (2) [34], where $\overline{\lambda}_p$ is the local slenderness of the considered plate element and can be determined from Eq. (3), in which f_{cr} is the elastic local buckling stress of the plate element, c is the width of the plate element excluding the corner radius, denoted as b_f and b_w for the flat widths of the flange and web, respectively, μ=0.3 is the Poisson's ratio, $\varepsilon=(235/f_y)^{0.5}$ is a material coefficient, and k_σ is the bucking factor, taken as 4 for internal webs in pure compression and $0.57-0.21\psi+0.07\psi^2$ for outstand flanges under stress gradients (with tips in compression), in which ψ is the end tensile to compressive stress ratio of the flat portion of the flange [34].

$$\rho=\begin{cases}(1-0.220/\overline{\lambda}_p)/\overline{\lambda}_p\le 1 & \overline{\lambda}_p>0.673 \text{ for internal elements}\\(1-0.188/\overline{\lambda}_p)/\overline{\lambda}_p\le 1 & \overline{\lambda}_p>0.748 \text{ for outstand elements}\end{cases} \tag{2}$$

$$\overline{\lambda}_p=\sqrt{\frac{f_y}{f_{cr}}}=\sqrt{\frac{f_y}{k_\sigma\frac{\pi^2E}{12(1-\mu^2)}(t/c)^2}}=\frac{c/t}{28.4\varepsilon\sqrt{k_\sigma}} \tag{3}$$

It is worth noting that EN 1993-1-12 [11] only covers the design of hot-rolled and welded steel structural members with material grades up to S700 and thus no design provisions can be directly applied to the studied press-braked (cold-formed) S960 UHSS channel section beams. In Section 4.1.2, the suitability of the Eurocode slenderness limits for hot-rolled and welded S690 HSS plate elements and cross-sections to their press-braked S960 UHSS counterparts was assessed, while evaluation of the EC3 predicted cross-section bending moment resistances for press-braked S960 UHSS channel section beams bent about the minor principal axes was made in Section 4.1.3.

4.1.2. Evaluation on current Eurocode Class 2 and 3 slenderness limits

The suitability of the current Eurocode Class 2 and 3 slenderness limits for internal elements in pure compression was evaluated, based on the test and FE data on press-braked S960 UHSS channel section beams bent about the minor principal axes in the 'n' orientation. The test and FE ultimate moments M_u, normalised by the corresponding cross-section plastic moment capacities M_{pl}, are plotted against the flat width-to-thickness ratios $c/t\varepsilon$ of the internal webs of the examined press-braked S960 UHSS channel section beams in Fig. 13, together with the Eurocode Class 2 slenderness limit for internal elements in compression ($c/t\varepsilon$=38). The results of the assessment revealed that the current Eurocode Class 2 slenderness limit for internal elements in compression well captures all the test and FE data points and thus can be used for the classification of the internal webs of press-braked S960 UHSS channel section beams in 'n'-orientation bending. A similar graphic evaluation was also carried out on the Eurocode Class 3 slenderness limit for internal elements in pure compression ($c/t\varepsilon$=42), as shown in Fig. 14, where the test and FE ultimate moments are now normalised by the cross-section elastic moment capacities. The evaluation results indicated that the current Eurocode Class 3 slenderness limit for internal elements in compression leads to safe but rather uneconomic classification results when used for the studied press-braked S960 UHSS channel section beams bent in the 'n' orientation.

The suitability of the current Eurocode Class 2 and 3 slenderness limits for outstand elements under stress gradients (with tips in compression) was assessed based on the experimental and FE ultimate moments of press-braked S960 UHSS channel section beams bent about the minor principal axes in the 'u' orientation. Figs 15 and 16 display the normalised test and FE ultimate moments (by the cross-section plastic moment capacities and elastic moment capacities, respectively) plotted against the ratios of $\alpha c/(t\varepsilon)$ and $c/(t\varepsilon k_\sigma^{0.5})$ of the outstand flanges of the studied press-braked S960 UHSS channel section beams, together with the corresponding

Eurocode Class 2 slenderness limit ($\alpha c/(t\varepsilon)$=10) and Class 3 slenderness limit ($c/(t\varepsilon k_{\sigma}^{0.5})$=21) for outstand elements under stress gradients (with tips in compression), where α is the ratio of the width of the compressive flat portion of the flange to the flat width of the flange. The Eurocode Class 2 slenderness limit for outstand elements under stress gradients (with tips in compression) was shown to be capable of accurately distinguishing Class 1 and Class 2 outstand flanges of press-braked S960 UHSS channel sections in 'u'-orientation bending from their Class 3 counterparts, while the corresponding Class 3 slenderness limit was found to be excessively conservative.

4.1.3. Comparisons of test and FE ultimate moments with EC3 resistance predictions

In this section, the accuracy of the EC3 design cross-section bending moment resistances for press-braked S960 UHSS channel section beams was assessed through comparing against the test and FE ultimate moments. Table 7 reports the mean ratios of the test and FE ultimate moments to the EC3 bending moment resistance predictions M_u/M_{EC3}. With regard to the 'u'-orientation bending cases, the EC3 predicted bending moment resistances were in good agreement with the test and FE ultimate moments for Class 1 and Class 2 channel sections, with the mean ratio M_u/M_{EC3} of 1.09 and the corresponding coefficient of variation (COV) of 0.05, whilst conservative yet consistent EC3 bending moment resistance predictions were obtained for Class 3 channel sections, with the mean M_u/M_{EC3} ratio of 1.78 and the COV of 0.04, and the EC3 design bending moment resistances were found to be rather conservative and scattered for Class 4 channel sections, with the mean M_u/M_{EC3} ratio equal to 2.23 and the COV equal to 0.21. In terms of the 'n'-orientation bending cases, the mean M_u/M_{EC3} ratios are equal to 1.06, 1.80 and 1.70, with the COVs of 0.03, 0.01, 0.04, for Class 1 (or Class 2), Class 3 and Class 4 channel sections, respectively, revealing that EN 1993-1-12 [11] yields precise and consistent predicted bending moment resistances for Class 1 and Class 2 channel section beams, but excessively conservative though still consistent bending moment resistance predictions for their Class 3 and Class 4 counterparts. It is also worth noting that the EC3 design bending moment resistances for press-braked S960 UHSS channel section beams bent in the ‘n’ orientation were generally more accurate and less scattered compared to those for press-braked S960 UHSS channel section beams in ‘u’-orientation bending; this is also evident in Fig. 17, in which the ratios of M_u/M_{EC3} are plotted against the flat width-to-thickness ratios of the most critical constituent plate elements of the channel sections, i.e. b_f/t for the ‘u’-orientation bending cases and b_w/t for the ‘n’-orientation bending cases.

4.2. AISI S100 and AS/NZS 4600

The North American Specification AISI S100 [12] and Australian/New Zealand Standard AS/NZS 4600 [13] were established for cold-formed steel members with material grades up to S690 and adopt the same design provisions for structural members in flexure. Both standards specify that the design bending moment resistance (M_{AISI} or $M_{AS/NZS}$) for a flexural member shall be taken as the minimum of the local, lateral-torsional and distortional buckling strengths. In the present study, the examined press-braked S960 UHSS channel section beams bent about the minor principal axes all failed by in-plane local buckling with no out-of-plane lateral-torsional and distortional deformations, and their design bending moment resistances were thus determined as the corresponding local buckling strengths. Given that in-plane local buckling failure of flexural members is specified by initiation of yielding in AISI S100 [12] and AS/NZS 4600 [13], the design bending moment resistances (M_{AISI} or $M_{AS/NZS}$) are respectively taken as the elastic moment capacities ($M_{el} = W_{el}f_y$) for non-slender sections and effective moment capacities ($M_{eff}=W_{eff}f_y$) for slender sections, where the effective section modulus W_{eff} is now determined using the AISI (or AS/NZS) effective width reduction factor, as defined by Eq. (4), where λ is the local slenderness of the plate element and calculated from Eq. (5), in which f is the maximum compressive stress in the considered plate element and derived by assuming a linear stress distribution over the plate element width with the yield stress at the extreme fibre. It is worth noting that f can be lower than the yield stress f_y for the internal webs of channel sections bent in the 'n' orientation, where the effective neutral axes are located farther from the extreme fibres (tips of the outstand flanges); this thus leads to lower plate element local slendernesses, compared to those determined by Eq. (3) in the Eurocodes, and consequently some Class 4 (slender) sections classified by EN 1993-1-12 [11] become non-slender sections when defined in accordance with AISI S100 [12] (or AS/NZS 4600 [13]). Moreover, AISI S100 [12] (or AS/NZS 4600 [13]) also provide an alternative simplified expression for calculating the plate buckling coefficient k_σ for outstand flanges under stress gradients (with tips in compression), as given by Eq. (6); note that the plate element local slendernesses, calculated based on the AISI (or AS/NZS) plate buckling coefficient, are also smaller than those derived from EN 1993-1-12 [11], indicating that EC3 Class 4 (slender) channel sections in 'u'-orientation bending may be defined as non-slender sections by AISI S100 [12] (or AS/NZS 4600 [13]).

$$\rho = \begin{cases} (1-0.22/\lambda)/\lambda \le 1 & \lambda > 0.673 \text{ for internal elements} \\ 0.925/\sqrt{\lambda} \le 1 & \lambda > 0.856 \text{ for outstand elements} \end{cases} \tag{4}$$

$$\lambda = \sqrt{\frac{f}{f_{cr}}} = \sqrt{\frac{f}{k_\sigma \dfrac{\pi^2 E}{12(1-\mu^2)}\left(t/c\right)^2}} \tag{5}$$

$$k_\sigma = 0.145\left(B_f/B_w\right) + 1.256 \quad \text{for } 0.1 \le B_f/B_w \le 1.0 \tag{6}$$

Quantitative and graphic comparisons of the cross-section bending moment resistances predicted by AISI S100 [12] (N_{AISI}) and AS/NZS 4600 [13] ($N_{AS/NZS}$) with the test and FE ultimate moments of press-braked S960 UHSS channel section beams were conducted, with the results presented in Table 8 and Fig. 18, respectively. The mean ratios of M_u/M_{AISI} (or $M_u/M_{AS/NZS}$) are equal to 1.71 and 1.04, with the COVs of 0.15 and 0.09, respectively for non-slender and slender channel section beams in 'u'-orientation bending, while the mean M_u/M_{AISI} (or $M_u/M_{AS/NZS}$) ratios are equal to 1.82 and 1.61, with the corresponding COVs equal to 0.05 and 0.01 for non-slender and slender channel section beams bent in the 'n' orientation. The results of the comparisons generally revealed that the American and Australian/New Zealand design approaches lead to accurate and consistent design bending moment resistances for slender S960 USS channel section beams in 'u'-orientation bending, but result in rather conservative design resistance predictions for all the other cases. Compared to EN 1993-1-12 [11], AISI S100 [12] and AS/NZS 4600 [13] were shown to yield much more conservative cross-section bending moment resistance predictions for non-slender S960 UHSS channel section beams, due to the neglect of plasticity (i.e. development of plastic moment capacities is not considered in the design of non-slender section flexural members in AISI S100 [12] and AS/NZS 4600 [13]), but more accurate and consistent design cross-section bending moment resistances for slender S960 UHSS channel section beams, owing mainly to the adoption of more relaxed (i.e. smaller) plate element local slendernesses and more accurate element width reduction factors.

Assessment of the codified design rules for structural members in flexure was also performed, based on the experimental data only, with the experimental to predicted ultimate moment ratios $M_{u,test}/M_{pred}$ for each press-braked S960 UHSS channel section beam specimen listed in Table 3. Overall, the three considered codified design approaches were all found to result in conservative bending moment resistance predictions for the tested S960 UHSS channel section beams bent about the minor principal axes. The mean ratios of $M_{u,test}/M_{pred}$ are equal to 1.26, 1.88 and 1.88, with the COVs of 0.27, 0.08 and 0.08 for the design bending moment resistances predicted from EN 1993-1-12 [11], AISI S100 [12] and AS/NZS 4600 [13], respectively. The assessment results also revealed that EN 1993-1-12 [11] yields more accurate but less consistent predicted bending moment resistances for the examined S960 UHSS channel section beam specimens than AISI S100 [12] and AS/NZS 4600 [13].

5. Conclusions

A comprehensive experimental and numerical study into the flexural behaviour and resistances of press-braked S960 UHSS channel section beams bent about the minor principal axes has been performed and presented. The experimental investigation included tensile flat and corner coupon tests, initial local geometric imperfection measurements and a total of 20 four-point bending beam tests bent about the minor principal axes in both the 'u' and 'n' orientations, while the numerical investigation comprised a simulation study to replicate the structural responses of the tested S960 UHSS channel beams and a parametric study to generate 113 FE data over a wide range of cross-section geometric sizes. The derived experimental and numerical data was firstly used to evaluate the applicability of the Eurocode Class 2 and 3 slenderness limits for hot-rolled and welded HSS plate elements to their cold-formed (press-braked) S960 UHSS counterparts, and then adopted to assess the accuracy of the bending moment resistance predictions obtained from EN 1993-1-12 [11], AISI S100 [12] and AS/NZS 4600 [13]. The assessment results generally revealed that the current Eurocode Class 2 slenderness limits yield accurate plate element (and thus cross-section) classifications of the studied press-braked S960 UHSS channel section beams, while the Class 3 slenderness limits appeared to be rather conservative. Regarding the design bending moment resistances, EN 1993-1-12 [11] was found to provide overall consistent and precise resistance predictions for Class 1 and Class 2 S960 UHSS channel sections in bending, but conservative and scattered predicted resistances for their Class 3 and Class 4 counterparts, whilst AISI S100 [12] and AS/NZS 4600 [13] were generally shown to yield rather scattered and excessively underestimated design bending moment resistances, except for slender S960 UHSS channel section beams in 'u'-orientation bending.

Acknowledgements

The authors would like to thank SSAB Swedish Steel Pte Ltd, Singapore and Vision One Pte Ltd for their assistances in fabricating press-braked S960 UHSS channel section beam specimens, and Mr Shao Quan Ong and Mr Jun Wei Toh for their help in the experiments as part of their undergraduate final year projects.

References

[1] Ma J-L, Chan T-M, Young B. Tests on high-strength steel hollow sections: a review. Pro ICE-Struct Build 2017;170(9):621–30.

[2] Pandey M, Young B. Compression capacities of cold-formed high strength steel tubular T-joints. J Constr Steel Res 2019;162:105650.

[3] Fang H, Chan T-M. Resistance of Axially Loaded Hot-finished S460 and S690 Steel Square Hollow Stub Columns at Elevated Temperatures. Structures. 2019;17:66-73.

[4] Li D, Huang Z, Uy B, Thai H T, Hou C. Slenderness limits for fabricated S960 ultra-high-strength steel and composite columns. Journal of Constructional Steel Research, 2019;159:109-121.

[5] Rasmussen K. High strength steel structures. Light Gauge Metal Structures Recent Advances: Springer; 2005. p. 121-41.

[6] Shi G, Zhou W, Lin C. Experimental investigation on the local buckling behavior of 960 MPa high strength steel welded section stub columns. Advances in Structural Engineering, 2015;18(3):423-437.

[7] Ma J-L, Chan T-M, Young B. Experimental investigation on stub-column behavior of cold-formed high-strength steel tubular sections. Journal of Structural Engineering (ASCE), 2015;142(5):04015174.

[8] Shi G, Ban H, Bijlaard FSK. Tests and numerical study of ultra-high strength steel columns with end restraints. Journal of Constructional Steel Research. 2012;70:236-47.

[9] Ban H, Shi G, Shi Y, Bradford MA. Experimental investigation of the overall buckling behaviour of 960MPa high strength steel columns. Journal of Constructional Steel Research. 2013;88:256-66.

[10] Ma J-L, Chan T-M, Young B. Experimental investigation of cold-formed high strength steel tubular beams. Engineering Structures. 2016;126:200-9.

[11] EN 1993-1-12. Eurocode 3: Design of steel structures – Part 1–12: Additional rules for the extension of EN 1993 up to steel grades S 700. Brussels (Belgium): CEN; 2007.

[12] AISI S100. North American specification for the design of cold-formed steel structural members. American Iron and Steel Institute; 2016.

[13] AS/NZS 4600. Cold-formed steel structures. Sydney: AS/NZS 4600:2018; 2018.

[14] SSAB. Bending of high strength steel-Strenx, Hardox and Docol. https://www.ssab.com/products/brands/strenx/products/strenx-960?accordion=downloads

[15] Wang F, Zhao O, Young B. Compressive behaviour and resistances of press-braked S960 ultra-high strength steel angle and channel sections. Engineering Structures. Under review.

[16] American Society for Testing and Materials (ASTM). Standard test methods for tension testing of metallic materials. E8/E8M-15a, West Conshohocken, PA., USA: ASTM International; 2015.

[17] Huang Y, Young B. The art of coupon tests. Journal of Constructional Steel Research, 2014;96:159-75.

[18] Li H-T, Young B. Tests of cold-formed high strength steel tubular sections undergoing web crippling. Engineering Structures, 2017;141:571-583.

[19] Wang F, Young B, Gardner L. Compressive testing and numerical modelling of concrete-filled double skin CHS with austenitic stainless steel outer tubes. Thin-Walled Structures. 2019;141:345-59.

[20] Schafer B, Peköz T. Computational modeling of cold-formed steel: characterizing geometric imperfections and residual stresses. Journal of constructional steel research. 1998;47:193-210.

[21] Chen M-T, Young B. Cross-sectional behavior of cold-formed steel semi-oval hollow sections. Engineering Structures, 2018;177:318-330.

[22] Liang Y, Zhao O, Long Y, Gardner L. Stainless steel channel sections under combined compression and minor axis bending–Part 1: Experimental study and numerical modelling. Journal of Constructional Steel Research, 2019, 152: 154-161.

[23] Sun Y, Zhao O. Material response and local stability of high-chromium stainless steel welded I-sections. Engineering Structures, 2019;178:212–26.

[24] Sun Y, Liang Y, Zhao O. Testing, numerical modelling and design of S690 high strength steel welded I-section stub columns. Journal of Constructional Steel Research. 2019;159:521-33.

[25] Zhao O, Gardner L, Young B. Buckling of ferritic stainless steel members under combined axial compression and bending. Journal of Constructional Steel Research. 2016;117:35-48.

[26] Chen M-T, Young B. Structural behavior of cold-formed steel semi-oval hollow section beams. Engineering Structures. 2019, 185: 400-411.

[27] Chan T-M, Gardner L. Bending strength of hot-rolled elliptical hollow sections. Journal of Constructional Steel Research, 2008, 64(9): 971–986.

[28] Zhao O, Rossi B, Gardner L, Young B. Experimental and numerical studies of ferritic stainless steel tubular cross sections under combined compression and bending. Journal of Structural Engineering. 2016;142.

[29] Zhao O, Rossi B, Gardner L, Young B. Behaviour of structural stainless steel cross-sections under combined loading – Part I: Experimental study. Engineering Structures. 2015;89:236-46.

[30] Wang F, Young B, Gardner L. Experimental study of square and rectangular CFDST sections with stainless steel outer tubes under axial compression. Journal of Structural Engineering. 2019;145.

[31] ABAQUS. ABAQUS/standard user’s manual. Version 6.17. Dassault Systemes Simulia Corp. USA; 2017.

[32] SSAB S960 channel section online brochure. https://www.ssab.com/products/steel-categories/open-sections/products/ssab-cold-formed-c-section

[33] EN 1993-1-1. Eurocode 3: Design of steel structures – Part 1–1: General rules and rules for buildings. Brussels (Belgium): CEN; 2005.

[34] EN 1993-1-5. Eurocode 3: Design of steel structures – Part 1–5: Plated structural elements. Brussels: European Committee for Standardization (CEN); 2015.

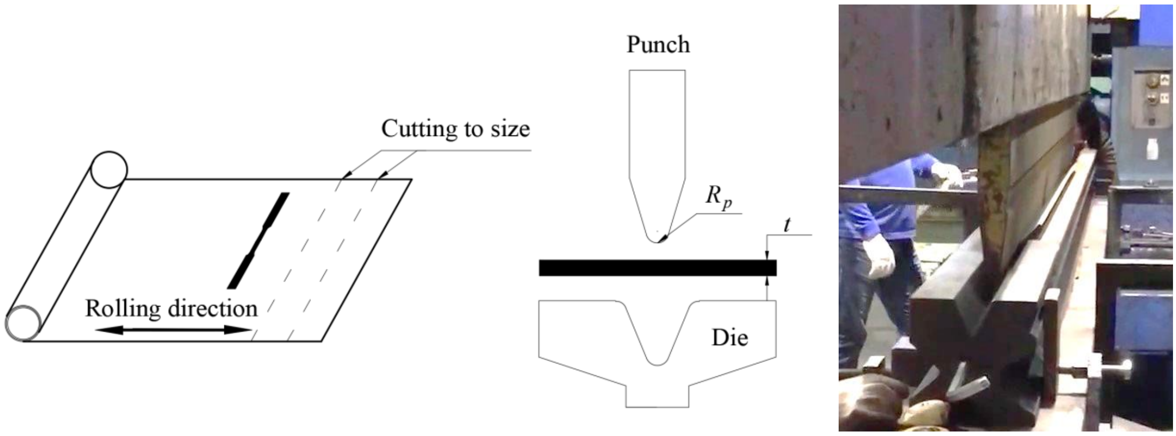

Fig. 1. Press-braking process of S960 UHSS channel section beam specimens.

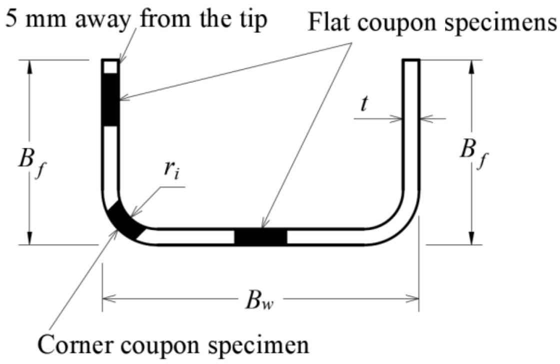

Fig. 2. Definition of symbols and locations of tensile coupons within cross-section.

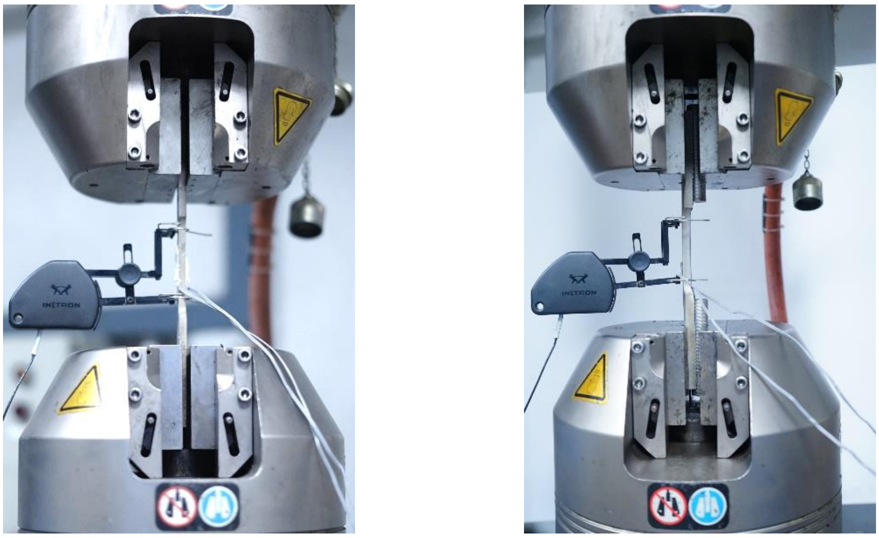

(a) Flat coupon test setup (b) Corner coupon test setup

Fig. 3. Tensile coupon test setups.

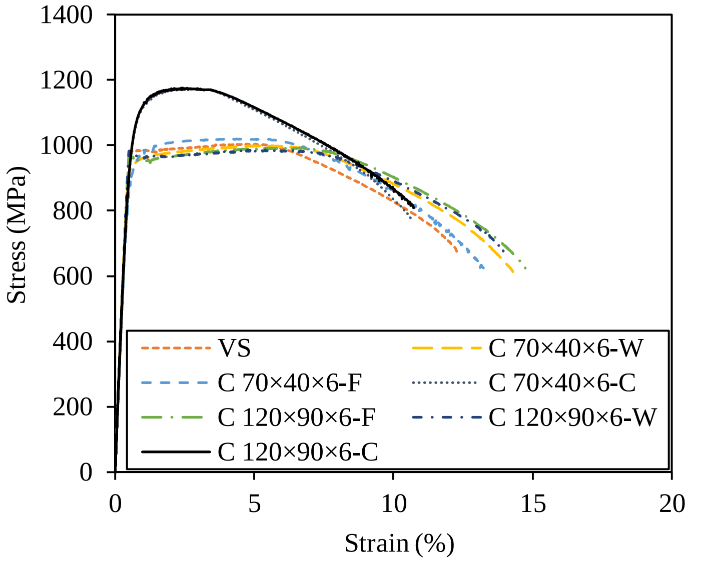

Fig. 4. Static stress–strain curves measured from tensile coupon tests [15].

Fig. 5. Test setup for initial local geometric imperfection measurements.

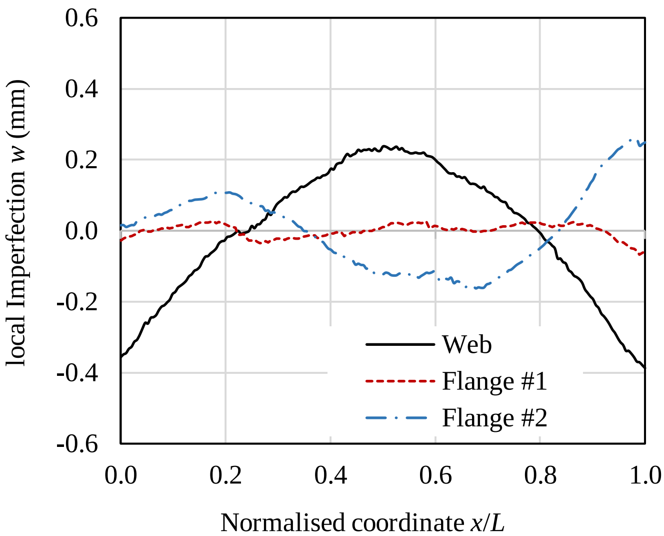

(a) C 80×45×6-u

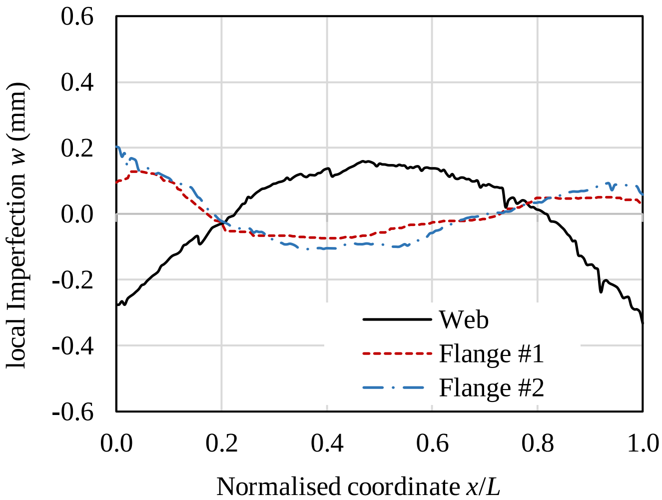

(b) C 80×45×6-n

Fig. 6 Measured initial local geometric imperfection distributions for typical press-braked S960 UHSS channel section beam specimens.

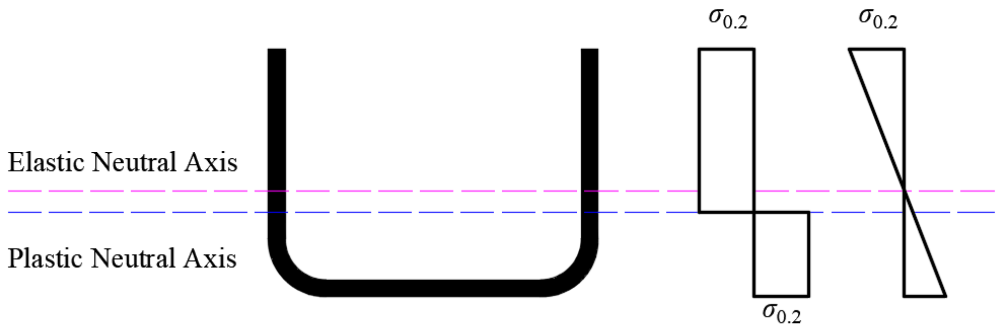

(a) Channel section bent in the ‘u’-orientation

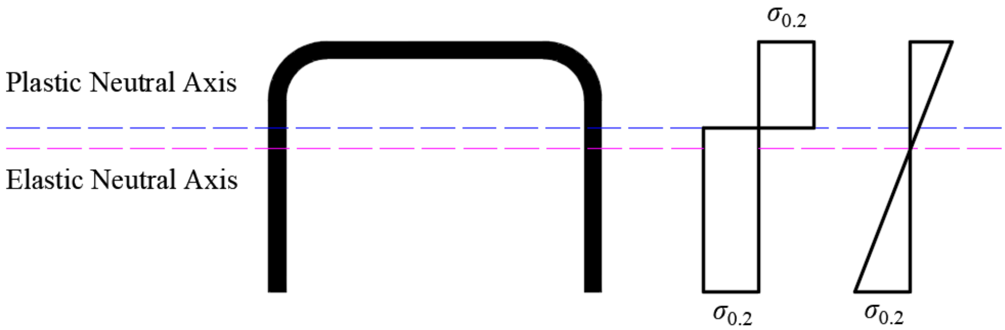

(b) Channel section bent in the ‘n’-orientation

Fig. 7. Elastic and plastic neutral axes of channel sections bent about the minor principal axes in the ‘u’ and ‘n’ orientations.

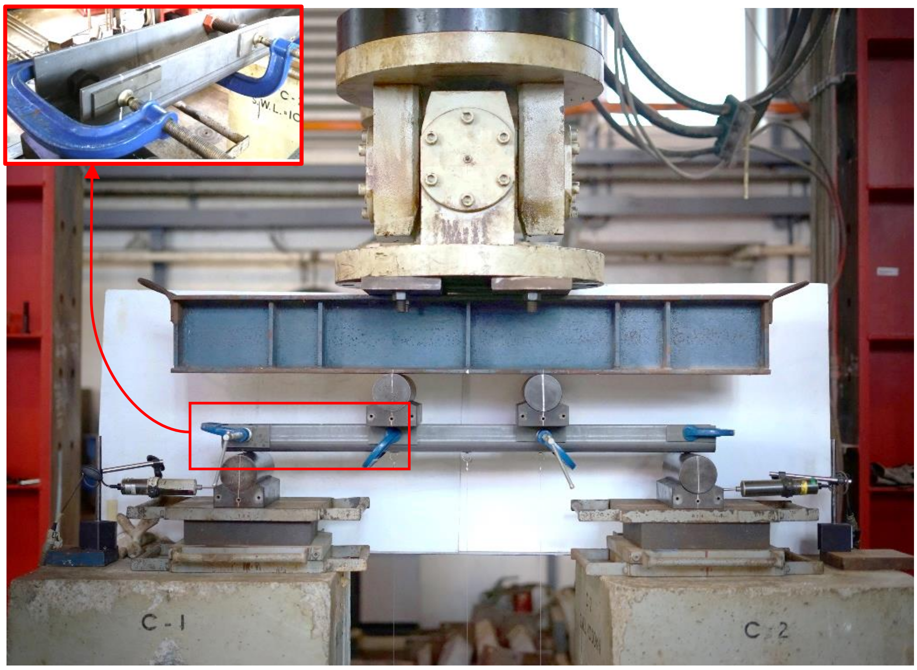

Fig. 8. Experimental setup for press-braked S960 UHSS channel section beams bent about the minor principal axes.

Fig. 9. Experimental and numerical failure modes for press-braked S960 UHSS channel section beam specimen C 120×90×6-u bent about the minor principal axis in the ‘u’ orientation.

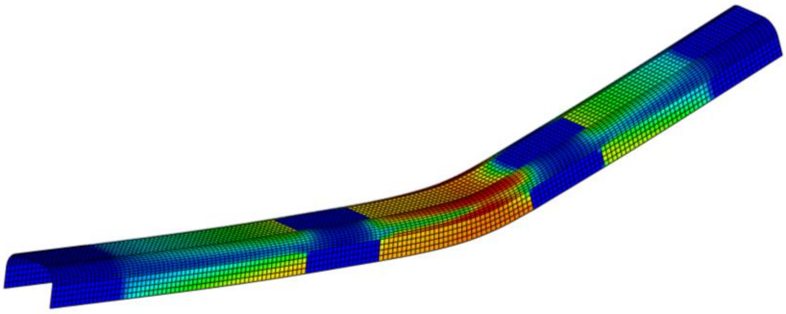

Fig. 10. Experimental and numerical failure modes for press-braked S960 UHSS channel section beam specimen C 80×45×6-n bent about the minor principal axis in the ‘n’ orientation.

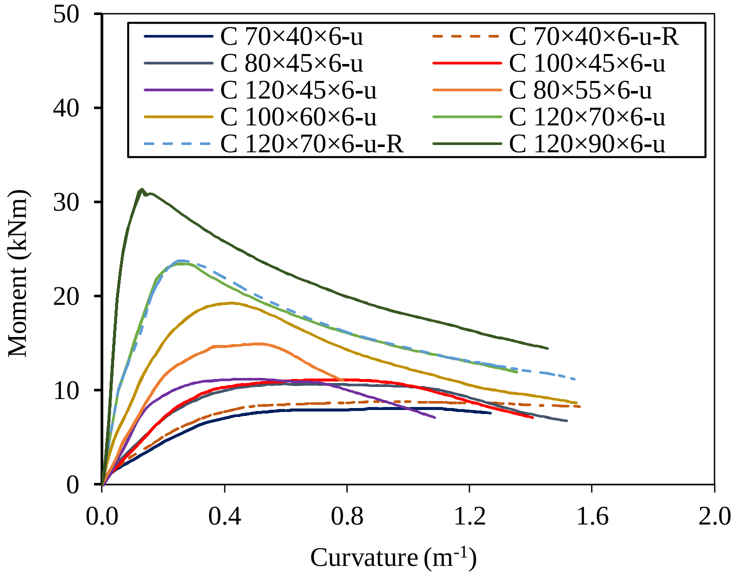

(a) Channel section beams bent in the ‘u’-orientation

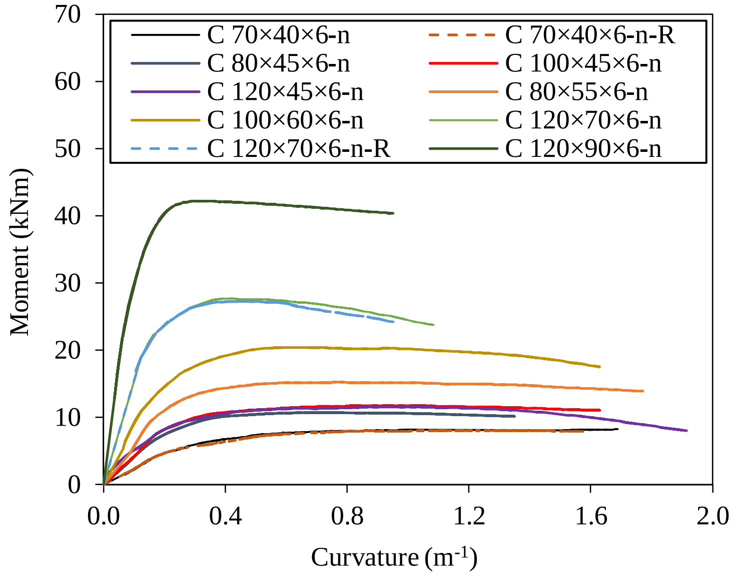

(b) Channel section beams bent in the 'n'-orientation

Fig. 11. Moment–curvature curves of the tested press-braked S960 UHSS channel section beam specimens in bending about the minor principal axes.

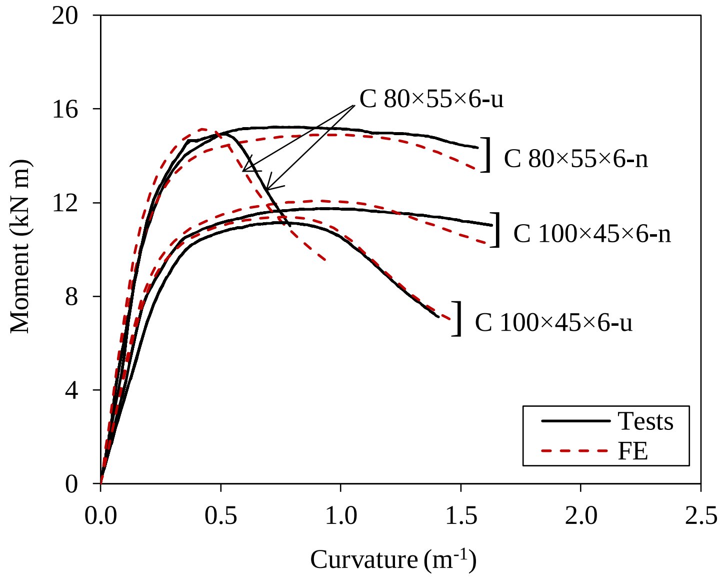

Fig. 12. Experimental and numerical moment–curvature curves for typical press-braked S960 UHSS channel section beam specimens.

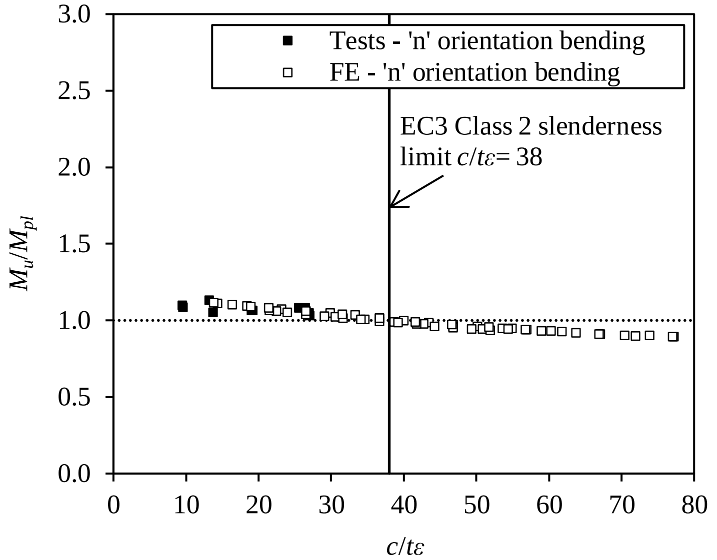

Fig. 13. Assessment of EC3 Class 2 slenderness limit for internal elements in compression.

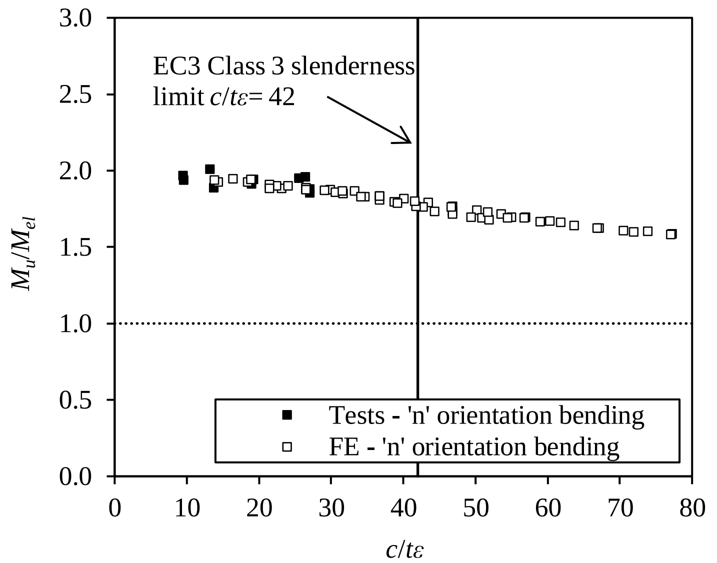

Fig. 14. Assessment of EC3 Class 3 slenderness limit for internal elements in compression.

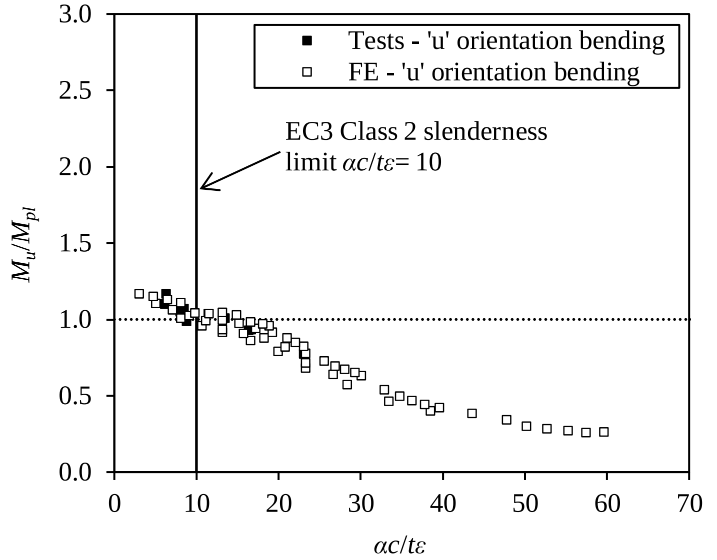

Fig. 15. Assessment of EC3 Class 2 slenderness limit for outstand elements under stress gradients (with tips in compression).

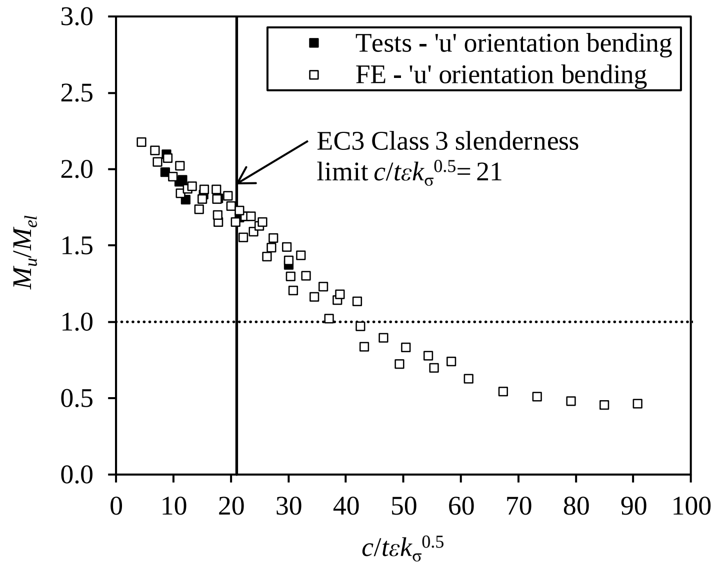

Fig. 16. Assessment of Class 3 slenderness limit for outstand elements under stress gradients (with tips in compression).

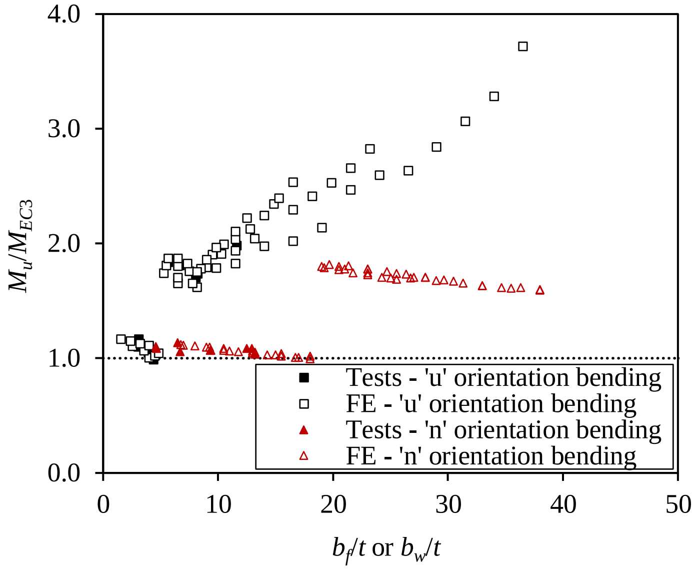

Fig. 17. Comparisons of test and FE ultimate moments with EN 1993-1-12 resistance predictions.

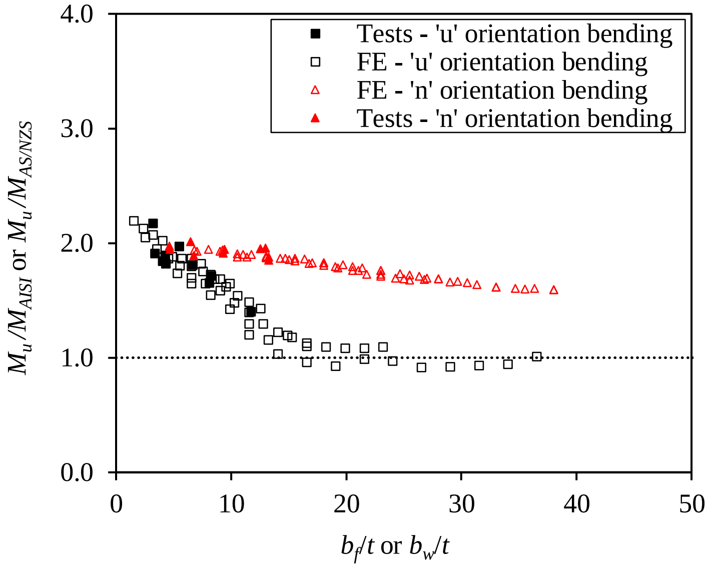

Fig. 18. Comparisons of test and FE ultimate moments with AISI S100 (and AS/NZS 4600) resistance predictions.

Table 1. Measured geometric dimensions and initial local geometric imperfections for the tested press-braked S960 UHSS channel section beam specimens.

Specimen ID	B_f (mm)	B_w (mm)	t (mm)	r_i (mm)	ω_w (mm)	ω_{f1} (mm)	ω_{f2} (mm)	ω_0 (mm)
C 70×40×6-u	40.00	72.57	6.15	14.8	0.50	0.11	0.10	0.50
C 70×40×6-u-R	39.51	71.47	6.13	14.8	0.42	0.24	0.28	0.42
C 70×40×6-n	39.92	69.29	6.03	14.8	0.52	0.18	0.11	0.52
C 70×40×6-n-R	40.81	69.37	6.00	14.8	0.56	0.41	0.01	0.56
C 80×45×6-u	45.80	80.93	6.03	14.5	0.39	0.07	0.26	0.39
C 80×45×6-n	46.18	81.66	6.06	14.5	0.33	0.13	0.20	0.33
C 100×45×6-u	45.25	101.06	6.17	14.8	0.08	0.13	0.17	0.17
C 100×45×6-n	46.10	100.28	6.20	14.8	0.12	0.10	0.12	0.12
C 120×45×6-u	46.59	120.38	6.01	14.5	0.33	0.28	0.19	0.33
C 120×45×6-n	46.33	120.62	6.02	14.5	0.32	0.20	0.18	0.32
C 80×55×6-u	55.41	79.89	6.12	14.8	0.35	0.10	0.12	0.35
C 80×55×6-n	53.69	80.48	6.03	14.8	0.35	0.15	0.10	0.35
C 100×60×6-u	61.82	99.10	6.19	14.5	0.20	0.30	0.16	0.30
C 100×60×6-n	61.74	99.05	6.20	14.5	0.07	0.15	0.36	0.36
C 120×70×6-u	70.39	120.93	6.17	14.5	0.04	0.16	0.13	0.16
C 120×70×6-u-R	70.32	119.66	6.05	14.5	0.08	0.28	0.15	0.28
C 120×70×6-n	70.46	120.23	6.03	15.0	0.03	0.12	0.15	0.15
C 120×70×6-n-R	70.58	119.04	6.14	15.0	0.10	0.18	0.35	0.35
C 120×90×6-u	91.79	120.38	6.09	15.0	0.04	0.15	0.33	0.33
C 120×90×6-n	91.11	121.55	6.01	15.0	0.05	0.16	0.18	0.18

Note: ‘R’ indicates a repeated specimen.

Table 2. Measured material properties of press-braked S960 UHSS channel sections from tensile coupon tests [15].

Coupon specimen ID	E (GPa)	f_y (MPa)	f_u (MPa)	ε_u (%)	ε_f (%)	f_u/f_y
VS	208	982	1011	5.1	12.3	1.03
C 70×40×6-W	214	935	1000	4.5	14.3	1.07
C 70×40×6-F	203	927	1021	5.1	13.3	1.10
C 70×40×6-C	203	1033	1173	2.4	10.6	1.13
C 120×90×6-W	208	969	994	4.7	13.9	1.03
C 120×90×6-F	200	963	1001	6.6	14.7	1.04
C 120×90×6-C	206	1030	1177	2.5	10.7	1.14

Table 3. Test results for press-braked S960 UHSS channel section beam specimens and codified flexural strength predictions.

Specimen ID	$M_{u,test}$ (kNm)	κ_f	$M_{u,test}/M_{pl}$	$M_{u,test}/M_{el}$	$M_{u,test}/M_{EC3}$	$M_{u,test}/M_{AISI}$	$M_{u,test}/M_{AS/NZS}$
C 70×40×6-u	8.85	0.92	1.10	2.18	1.17	2.18	2.18
C 70×40×6-u-R	8.09	0.93	1.09	1.91	1.10	1.91	1.91
C 70×40×6-n	8.03	1.69	1.17	1.98	1.10	1.98	1.98
C 70×40×6-n-R	8.23	1.35	1.10	1.95	1.09	1.95	1.95
C 80×45×6-u	10.75	0.61	1.06	1.90	1.07	1.90	1.90
C 80×45×6-n	10.76	0.72	1.07	1.89	1.06	1.89	1.89
C 100×45×6-u	11.15	0.74	1.07	1.85	1.05	1.85	1.85
C 100×45×6-n	11.75	0.99	1.05	1.95	1.07	1.95	1.95
C 120×45×6-u	11.21	0.48	1.03	1.82	0.99	1.82	1.82
C 120×45×6-n	11.57	0.92	0.99	1.88	1.03	1.88	1.88
C 80×55×6-u	14.96	0.52	1.13	1.98	1.84	1.98	1.98
C 80×55×6-n	15.23	0.79	1.04	2.01	1.13	2.01	2.01
C 100×60×6-u	19.36	0.43	1.07	1.81	1.81	1.81	1.81
C 100×60×6-n	20.43	0.59	1.01	1.91	1.07	1.91	1.91
C 120×70×6-u	23.98	0.30	1.09	1.72	1.70	1.72	1.72
C 120×70×6-u-R	23.60	0.33	1.08	1.66	1.74	1.66	1.66
C 120×70×6-n	27.35	0.39	0.93	1.96	1.09	1.96	1.96
C 120×70×6-n-R	27.74	0.44	0.94	1.95	1.08	1.95	1.95
C 120×90×6-u	32.10	0.15	1.05	1.41	1.99	1.41	1.41
C 120×90×6-n	42.30	0.32	0.78	1.85	1.05	1.85	1.85
Mean			1.04	1.88	1.26	1.88	1.88
COV			0.08	0.08	0.27	0.08	0.08

Table 4. Comparison of four-point bending test ultimate moments with FE ultimate moments for varying imperfection amplitudes.

Specimen ID	$M_{u,FE}/M_{u,test}$				
	ω_0	$t/100$	$t/50$	$t/25$	$t/10$
C 70×40×6-u	0.98	0.98	0.98	0.97	0.96
C 70×40×6-u-R	1.03	1.04	1.03	1.02	1.02
C 70×40×6-n	1.05	1.05	1.05	1.04	1.04
C 70×40×6-n-R	1.06	1.06	1.06	1.06	1.05
C 80×45×6-u	1.02	1.03	1.03	1.02	1.00
C 80×45×6-n	1.06	1.06	1.06	1.06	1.06
C 100×45×6-u	1.02	1.02	1.02	1.02	1.00
C 100×45×6-n	1.03	1.03	1.03	1.03	1.03
C 120×45×6-u	1.04	1.05	1.05	1.04	1.02
C 120×45×6-n	1.03	1.03	1.03	1.03	1.03
C 80×55×6-u	1.01	1.05	1.04	1.03	0.99
C 80×55×6-n	0.98	0.98	0.98	0.98	0.98
C 100×60×6-u	0.98	1.02	1.01	0.99	0.94
C 100×60×6-n	1.02	1.02	1.02	1.02	1.02
C 120×70×6-u	0.98	1.00	0.99	0.96	0.90
C 120×70×6-u-R	0.99	0.99	0.98	0.97	0.94
C 120×70×6-n	0.97	0.97	0.97	0.97	0.97
C 120×70×6-n-R	0.98	0.98	0.98	0.98	0.98
C 120×90×6-u	1.06	0.99	1.01	1.02	1.08
C 120×90×6-n	1.01	1.01	1.01	1.01	1.01
Mean	1.02	1.02	1.02	1.01	1.00
COV	0.03	0.03	0.03	0.03	0.05

Table 5. Cross-section dimensions of channel section beams in 'u'-orientation bending selected for parametric studies.

Bending orientation	t (mm)	B_w (mm)	B_f (mm)
'u'-orientation bending	4	180	60, 70, 80, 90, 100, 110, 120, 130, 140, 150, 160
	6	180	60, 70, 80, 90, 100, 110, 120, 130, 140, 150, 160
	8	180	60, 70, 80, 90, 100, 110, 120, 130, 140, 150, 160
	10	180	60, 70, 80, 90, 100, 110, 120, 130, 140, 150, 160
	12	180	60, 70, 80, 90, 100, 110, 120, 130, 140, 150, 160

Table 6. Cross-section dimensions of channel section beams in 'n'-orientation bending selected for parametric studies.

Bending orientation	t (mm)	B_f (mm)	B_w (mm)
'n'-orientation bending	6	90	110, 120, 130, 140, 150, 160, 170, 180, 190, 200, 210, 220, 230, 240, 250, 260, 270
	8	90	110, 120, 130, 140, 150, 160, 170, 180, 190, 200, 210, 220, 230, 240, 250, 260, 270
	4	60	70, 80, 90, 100, 110, 120, 130, 140, 150, 160, 170, 180
	5	60	70, 80, 90, 100, 110, 120, 130, 140, 150, 160, 170, 180

Table 7. Comparisons of test and FE ultimate moments with predicted bending moment resistances from EN 1993-1-12 [11].

Bending orientation	Section classification	No. of data		M_u/M_{EC3}	
		Test	FE	Mean	COV
'u'-orientation bending	Class 1 or 2	5	9	1.09	0.05
	Class 3	2	10	1.78	0.04
	Class 4	3	36	2.23	0.21
	Subtotal	10	55	1.90	0.31
'n'-orientation bending	Class 1 or 2	10	25	1.06	0.03
	Class 3	0	5	1.80	0.01
	Class 4	0	28	1.70	0.04
	Subtotal	10	58	1.38	0.24
Total		20	113	1.63	0.33

Table 8. Comparisons of test and FE ultimate moments with predicted bending moment resistances from AISI S100 [12] or AS/NZS 4600 [13].

Bending orientation	Section classification	No. of data		M_u/M_{AISI} or $M_u/M_{AS/NZS}$	
		Test	FE	Mean	COV
'u'-orientation bending	Non-slender	10	37	1.71	0.15
	Slender	0	18	1.04	0.09
	Subtotal	10	55	1.52	0.25
'n'-orientation bending	Non-slender	10	51	1.82	0.05
	Slender	0	7	1.61	0.01
	Subtotal	10	58	1.80	0.06
Total		20	113	1.67	0.19